Journal of Nuclear Materials 178 (1991) 33–39
North-Holland

High temperature X-ray diffraction study of the U_4O_9 formation on UO_2 sintered plates

Silvio Rainho Teixeira [b] and Kengo Imakuma [a]

[a] *Instituto de Pesquisas Energéticas e Nucleares, Comissão Nacional de Energia Nuclear, Caixa Postal 11049, 01000 São Paulo, SP, Brazil*

[b] *UNESP – FCT, Caixa Postal 957, 19060 Presidente Prudente, SP, Brazil*

Received 22 August 1990; accepted 22 October 1990

The surface oxidation of UO_2 sintered plates at 170–275 °C was studied in situ by high temperature X-ray diffractometry. At very low oxygen concentration, UO_2 is oxidized to U_4O_9, while at 300 °C and argon–20 vol% oxygen it is oxidized up to U_3O_7. X-ray diffraction profiles of the UO_2, U_4O_9 and U_3O_7 phases were well characterized during the transformations. The activation energy for the transformation of UO_2 to U_4O_9, obtained from X-ray diffraction data, was found to be 117 ± 9 kJ/mol and 90 ± 14 kJ/mol for the β-(311) and α-(200) reflections, respectively.

1. Introduction

The oxidation of UO_2 pellets and powders has been widely studied [1–13]. The kinetic behavior of UO_2 following the formation of intermediate metastable phases, has also been intensively investigated.

It is generally accepted [6] that the oxidation of UO_2 proceeds in two steps: firstly, to a tetragonal phase of composition U_3O_7 in the parabolic form, and then, to U_3O_8 in the S-shaped form. Although the existence of the UO_2, U_4O_9, U_3O_7 and U_3O_8 phases is well established, several papers [6,9,12,13] regarding the UO_2 surface oxidation, at low temperature, did not distinguish the U_4O_9 phase during the UO_2–U_3O_7 oxidation. Taylor [9] asserted that no information was obtained on the presence of $UO_{2.35}$ (U_4O_9), and he derived the activation energy for the oxidation of UO_2 to β-$UO_{2.33}$ (U_3O_7) from X-ray data. The kinetic investigation of the progress of the UO_2 oxidation by continuous monitoring of the formation of the intermediate phases by high temperature diffractometry is still lacking in the literature.

Since the structure of the oxides varies continuously with composition, it is possible to follow the kinetic reaction by measuring the changes in the Bragg reflection intensities and also to observe the change in the reflection positions of the phases due to oxygen absorption.

The purpose of this study is to follow in situ alterations observed in the UO_2 X-ray diffractograms due to its reaction with oxygen. With these informations we wish to identify the phases formed during the oxidation, and to evaluate the oxidation kinetics of the UO_2–U_4O_9 transformation.

2. Experimental

2.1. Specimens

The UO_2 samples were prepared by IPEN's Nuclear Metallurgical Center in the following steps: calcination of ammonium diuranate (ADU) at 700 °C for 3 h to form U_3O_8 and reduction under hydrogen atmosphere at 700 °C for 1.5 h, to UO_2. The pellets (40 mm diameter) were compacted and sintered to a final density of 10.5 g/cm^3. The samples were cut to form plates of $23 \times 15 \times 1.2$ mm and then the surface to be studied was polished. The main impurities detected by a spectrographic method were (in ppm) Si(82), Al(200), Cr(12), Ni(6), Mn(3.6), Cu(0.9), B(0.1), Pb(< 1), Sn(< 1), Bi(< 1), V(< 3), Mg(< 2.4), Cd(< 0.1), P(< 55), Mo(< 2), Zn(< 10) and Fe($\simeq$ 20).

2.2. Diffractometry

A commercial goniometer (Rigaku-Geigerflex) equipped with a step scanning system and a high-temperature chamber was used to perform the line profile measurements. The experimental setting of step scanning was 0.02° and the time fixed for counts was 20 s. The reflections were measured with Cu K_α and Cu K_β radiations. The high-temperature chamber was equipped with a platinum resistance furnace and a Pt/Pt–13% Rh thermocouple.

The stages of oxidation were characterized by measuring the peak position (2θ) and the integrated intensity for each reflection (hkl), for each phase. Afterwards, the samples were ground and analysed in a Guinier–Hägg chamber.

Fig. 1 shows the α-(200) and β-(311) line profiles of UO_2 (disappearing) and U_4O_9 (appearing) during isothermal treatment at 235 °C.

2.3. Kinetics

The kinetic study was performed under a continuous flow of argon (with $\simeq 150$ ppm O_2) in three series of isothermal heat treatments: 170, 235 and 275 ± 5 °C. The (200) reflection was measured with Cu $K\alpha$ radiation and the (311) reflection with Cu K_β radiation.

The fraction of conversion f from UO_2 to U_4O_9 was obtained by means of the following equation (1):

$$f = \frac{I(U_4O_9)}{I(UO_2) + I(U_4O_9)}, \tag{1}$$

where $I(U_4O_9)$ and $I(UO_2)$ are the integrated intensities of the (hkl) reflections of the U_4O_9 and UO_2 phases, respectively. The f values were calculated for the same (hkl) reflection of UO_2 (fcc) and U_4O_9 (fcc). The integrated intensity values were obtained by the ANACRON [14] package with the step scanning data.

The rate constants k were obtained by using the following rate equations [6]:

$$\left[1 - (1-f)^{1/3}\right]^2 = kt, \tag{2}$$

$$1 - \tfrac{2}{3}f - (1-f)^{2/3} = kt, \tag{3}$$

where t is the time, k is the rate constant which includes the diffusion coefficient of oxygen in U_4O_9. These equations are used when the diffusion of oxygen through a surface layer of a new phase (U_4O_9), on the matrix (UO_2), is the rate-controlling process.

The activation energy is obtained by means of eq. (4), from the Arrhenius plot k versus $(1/T)$.

$$k = k_0 \exp(-Q/RT). \tag{4}$$

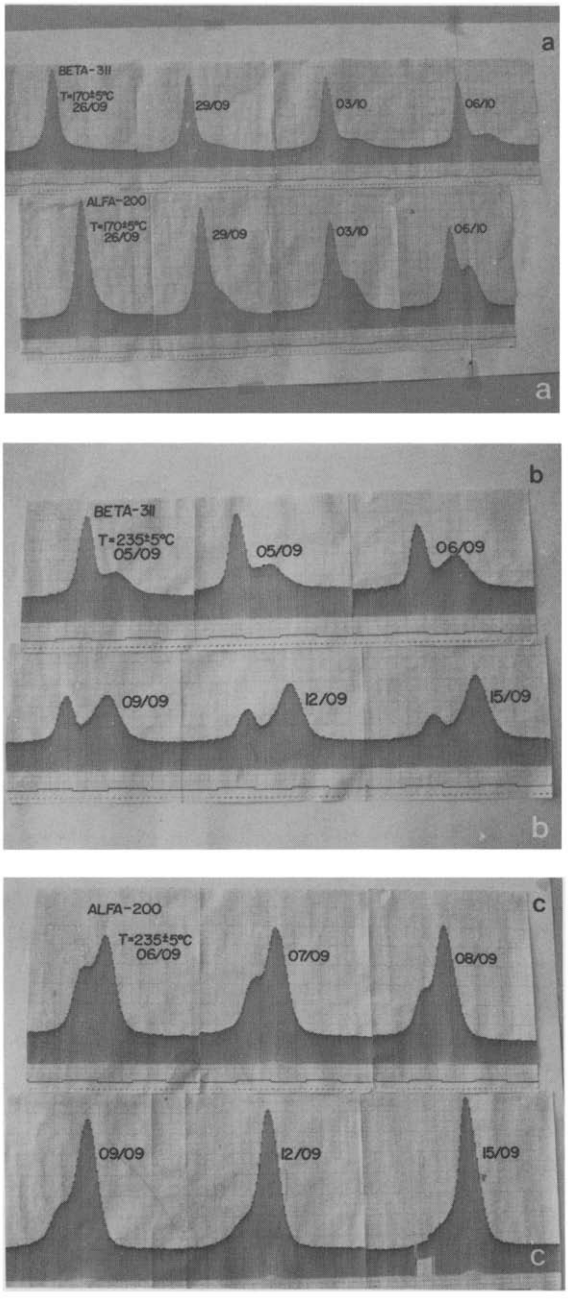

Fig. 1. The α-(200) and β-(311) diffraction peaks of UO_2 (left) and U_4O_9 (right) during isothermal oxidation at 170 °C (a) and 235 °C (b) and (c). (The first number means the day and the second the month).

3. Results and discussion

3.1. Thermal expansion

The behavior of the lattice parameter a_0 as a function of temperature of IPEN's UO_2 and Gronvold's [3] samples ($UO_{2.00}$, $UO_{2.05}$ and $UO_{2.10}$) were compared. The composition (O/U) of UO_2 (IPEN) ranged from 2.05 to 2.10 and its average linear thermal expansion coeficient (10.5×10^{-6} K^{-1}) is in good agreement with the literature [2,3,11].

3.2. Phase relationships

Even though some papers [1,5,6,9,10,12,13] indicate the direct oxidation of UO_2 (fcc) to U_3O_7 (tetragonal), at low oxidation temperature, in this work the formation of the U_4O_9 (fcc) phase was observed before the U_3O_7 (tetragonal) phase appeared.

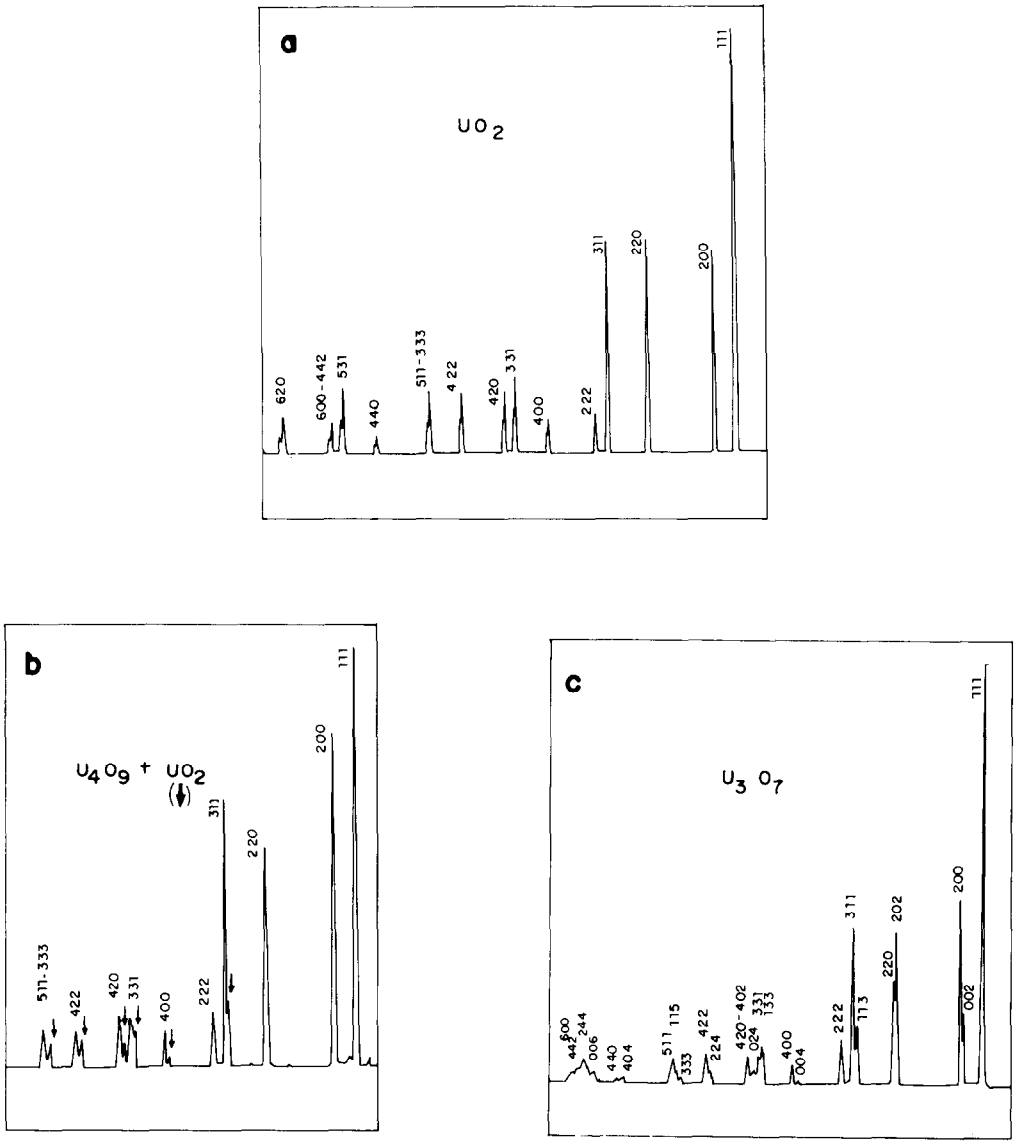

Fig. 2. Diffraction patterns of the observed phases: (a) UO_2, (b) $U_4O_9 + UO_2$ (after 290 h at 235 °C) and (c) U_3O_7.

Fig. 2 shows the diffraction patterns of UO_2, U_4O_9 + UO_2 (after 290 h at 235 °C) and U_3O_7. The last pattern was obtained by raising the temperature (to 300 °C) and the oxygen concentration (to 20 vol%) of the argon gas. Fig. 3 shows the UO_2 (disappearing) to U_4O_9 (appearing), and U_4O_9 (disappearing) to U_3O_7 (appearing) transformations for the β-(311) (fig. 3b) and β-(220) (fig. 3a) reflections . Fig. 4 presents the α-(200, 220, 311, 422, 511) step-scanning reflections of the two phases after 290 h at 235 °C. A diffraction peak (*hkl*), observed with a parafocussing diffractometer, is generated solely by crystallites with the (*hkl*) plane parallel to the sample surface. Using the high temperature chamber, the sample stand is fixed during the

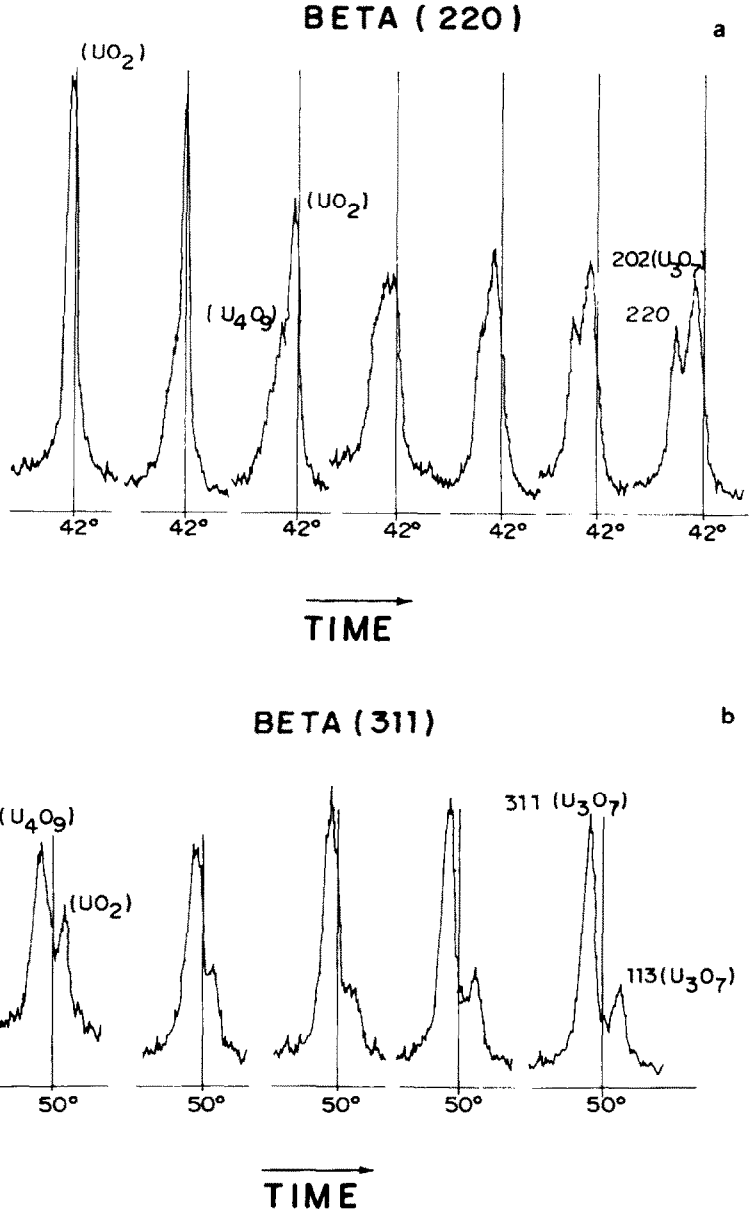

Fig. 3. Changes in (a) β-(220) and (b) β-(311) X-ray diffraction profiles during the UO_2 (fcc) to U_4O_9 (fcc) and to U_3O_7 (tetragonal transformation (temperature and oxygen concentration not constant).

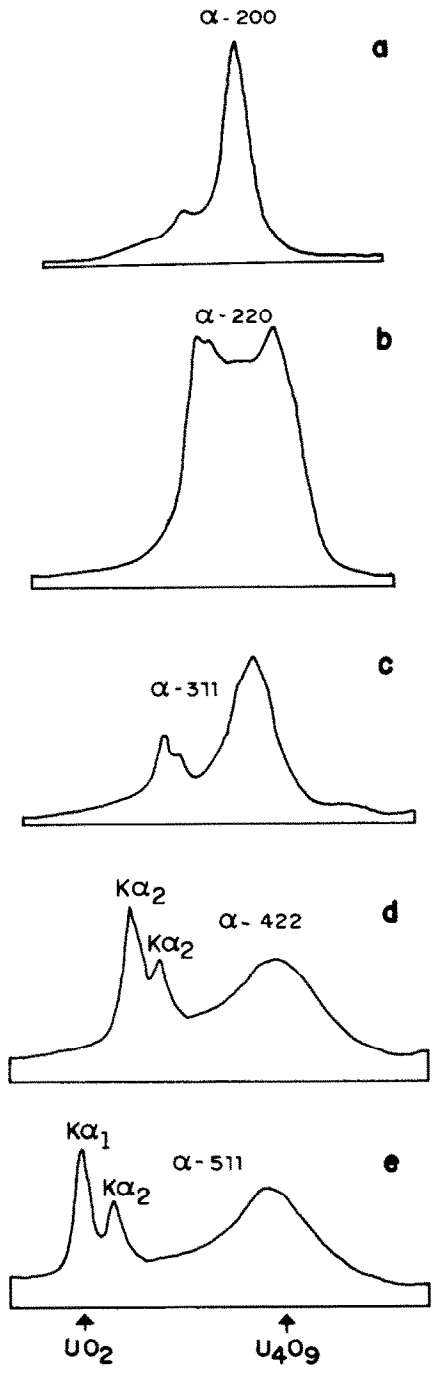

Fig. 4. Comparison of (a) (200), (b) (220), (c) (311), (d) (422) and (e) (511) α-reflections, after 290 h at 235 °C.

Table 1
Lattice parameters (at 20 ± 2 °C) in nm of the samples before and after oxidation (Guinier Hägg chamber)

Phase	Before oxidation	After oxidation
UO_2	0.5474 ± 0.0003	0.5472 ± 0.0003
U_4O_9	–	0.5453 ± 0.0003
U_3O_7	–	$a = 0.5401 \pm 0.0004$ $c = 0.5506 \pm 0.0004$

exposure time and so is the studied area of the sample. Therefore, the corresponding UO_2 and U_4O_9 peaks arise from the same grains. In figs. 2–4, a distinct behavior of each (*hkl*) reflection can be observed during the UO_2–U_4O_9 transformation. This indicates a preferential direction of U_4O_9 phase growth into the UO_2 phase.

The lattice parameters obtained by use of the Guinier–Hägg chamber are presented in table 1.

From figs. 2–4 it can be derived that the transformation occurs in the following way: (1) the diffracted intensities of UO_2 decrease while the corresponding U_4O_9 intensities increase, (2) the tetragonal U_3O_7 phase is characterized by the appearance of triplets like (333, 511 + 151, 115), doublets like (311 + 131, 113) and singlets of the type (*hhh*) after the U_4O_9 formation. (3) Finally, the gaps between the U_3O_7 doublets increase during the isothermal treatment, as does the c/a ratio.

3.3. Oxidation kinetics

The fraction f of UO_2 converted to U_4O_9 is represented as a function of the reaction time in fig. 5. The parabolic form of the rate curves characterizes the nature of the oxidation kinetics, which is predominantly controlled by oxygen diffusion through the U_4O_9 product layer. As the diffusion of oxygen through the U_4O_9

Table 2
Activation energies obtained by different techniques

Activation energie (kJ/mol)	Technique
113	ref. [6]
75–113	ref. [6]
105–126	ref. [6]
110	refs. [1,6]
103	ref. [6]
112	ref. [9]
117 ± 9	to β-311 [a]
90 ± 14	to α-200 [a]

[a] Mean value from eqs. (2) and (3).

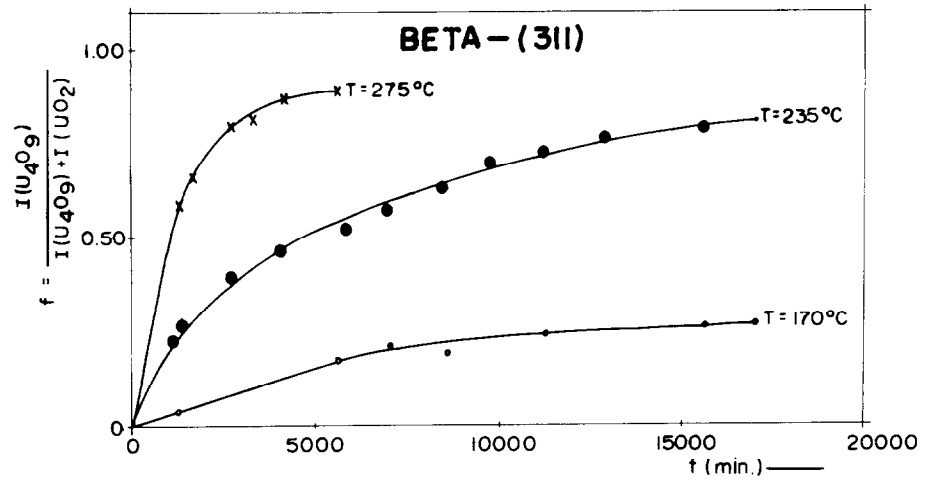

Fig. 5. Rate curves for the relative concentration f of U_4O_9 (β-(311) reflection).

(fcc) phase is the rate-controlling process, the rate eqs. (2) and (3) were used. It must be remarked, however, that the rate constant (k) in eqs. (2) and (3) is defined for the spherical diffusion problem and, therefore, the application to the present problem (plates) is only an approximation. The eqs. (2) and (3) (and $f^2 = kt$) give similar activation energies. These equations were used to normalize the kt values and to test the validity of the results by comparing the activation energies obtained from Arrhenius plots (ln k versus $1/T$), figs. 6 and 7,

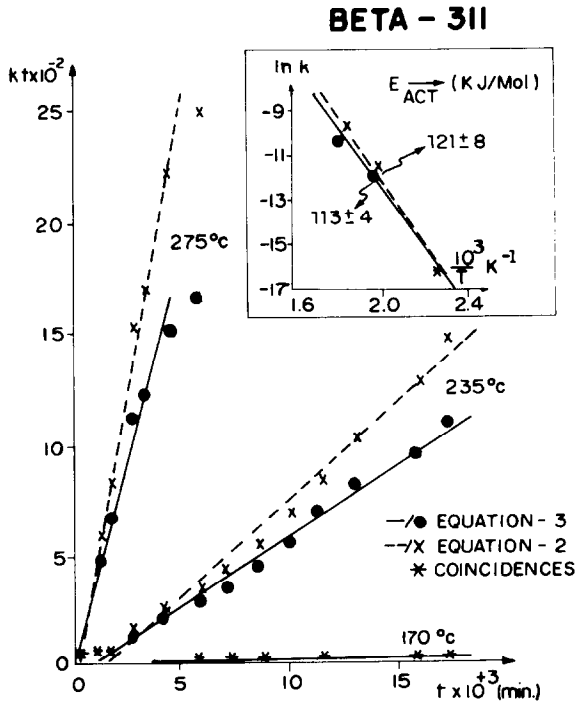

Fig. 6. Plots of kt (eqs. (2) and (3)) versus time and Arrhenius plot for β-(311) reflection.

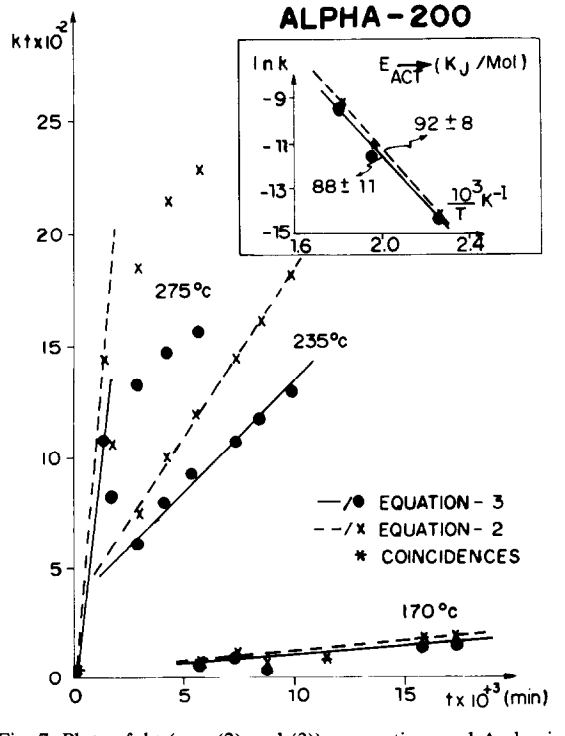

Fig. 7. Plots of kt (eqs. (2) and (3)) versus time and Arrhenius plot for α-(200) reflection.

with values obtained by different techniques, table 2. The values for the rate constants k for the oxidation process were obtained from fig. 6 (for β-(311)) and from fig. 7 (for α-(200)). These figures also show the respective Arrhenius plots in which both eqs. (2) and (3) were used. The values of the activation energies (table 2) obtained from Arrhenius plots are in good agreement with those obtained by other authors for the oxidation of UO_2 to U_3O_7, using different techniques (TGA, measurement of diffusion coefficients and X-ray diffraction).

4. Conclusions

The formation of U_4O_9 by oxidation of IPEN UO_2 fuel (plates) at 170–275 °C has observed in situ by high temperature X-ray diffractometry. The oxidation of UO_2 was followed up to the U_3O_7 phase and proceeds in the following sequence: $UO_2 \rightarrow U_4O_9 \rightarrow U_3O_7$. These three phases was identified by X-ray diffraction techniques (diffractometer and Guinier–Hägg chamber). The activation energies for the oxidation of UO_2 to U_4O_9 from X-ray data are: 117 ± 9 kJ/mol and $90 + 14$ kJ/mol for the β-(311) and α-(200) reflections, respectively. These values are in good agreement with literature data [1,6,9].

Acknowledgments

This research was partly sponsored by the Comissão Nacional de Energia Nuclear – CNEN.

References

[1] S. Aronson, R.B. Roof and J. Belle, J. Chem. Phys. 27 (1957) 137.
[2] J. Belle, Uranium Dioxide, Properties and Nuclear Applications (USAEC, 1961).
[3] F. Gronvold, J. Inorg. Nucl. Chem. 1 (1955) 357.
[4] H. Ohashi, E. Noda and T. Morozumi, J. Nucl. Sci. Technol. 11 (1974) 445.
[5] H.R. Hoekstra, A. Santoro and S. Siegel, J. Inorg. Nucl. Chem. 18 (1961) 166.
[6] Y. Saito, in: Proc. US–Japan Joint Seminar on Defects and Diffusion in Solids, Tokyo, October 4–6, 1976, p. 33–44.
[7] D.A. Dominey, J. Inorg. Nucl. Chem. 30 (1968) 1557.
[8] M. Iwasaki and N. Ishikawa, J. Nucl. Mater. 36 (1970) 116.
[9] P. Taylor, E.A. Burgess and D.G. Owen, J. Nucl. Mater. 88 (1980) 153.
[10] N. Masaki, J. Nucl. Mater. 101 (1981) 229.
[11] International Atomic Energy Agency, Thermodynamic and Transport Properties of Uranium Dioxide and Related Phases, IAEA Technical Report Series 39 (1965).
[12] G.C. Allen, Philos Mag. B51 (1985) 465.
[13] G.C. Allen, P.A. Tempest and J.W. Tyler, J. Chem. Soc. Faraday Trans. I 84 (1988) 4061.
[14] ANACRON – Programa Computacional para a Análise de Cromatogramas, Instituto de Pesquisas Energeticas e Nucleares (IPEN), São Paulo, Brazil, IPEN Informativo 5 (January 1981).